



Deposited via The University of Leeds.

White Rose Research Online URL for this paper:

<https://eprints.whiterose.ac.uk/id/eprint/167102/>

Version: Accepted Version

Article:

Xia, D, Huang, P, Li, H et al. (2020) Fast and Efficient Electrical-Thermal Responses of Functional Nanoparticles Decorated Nanocarbon Aerogels. *Chemical Communications*. ISSN: 1359-7345

<https://doi.org/10.1039/d0cc03784b>

This item is protected by copyright, all rights reserved. This is an author produced version of an article published in *Chemical Communications*. Uploaded in accordance with the publisher's self-archiving policy.

Reuse

Items deposited in White Rose Research Online are protected by copyright, with all rights reserved unless indicated otherwise. They may be downloaded and/or printed for private study, or other acts as permitted by national copyright laws. The publisher or other rights holders may allow further reproduction and re-use of the full text version. This is indicated by the licence information on the White Rose Research Online record for the item.

Takedown

If you consider content in White Rose Research Online to be in breach of UK law, please notify us by emailing eprints@whiterose.ac.uk including the URL of the record and the reason for the withdrawal request.

ChemComm

Chemical Communications

Accepted Manuscript

This article can be cited before page numbers have been issued, to do this please use: D. Xia, P. Huang, H. Li and N. Rubio Carrero, *Chem. Commun.*, 2020, DOI: 10.1039/D0CC03784B.



This is an Accepted Manuscript, which has been through the Royal Society of Chemistry peer review process and has been accepted for publication.

Accepted Manuscripts are published online shortly after acceptance, before technical editing, formatting and proof reading. Using this free service, authors can make their results available to the community, in citable form, before we publish the edited article. We will replace this Accepted Manuscript with the edited and formatted Advance Article as soon as it is available.

You can find more information about Accepted Manuscripts in the [Information for Authors](#).

Please note that technical editing may introduce minor changes to the text and/or graphics, which may alter content. The journal's standard [Terms & Conditions](#) and the [Ethical guidelines](#) still apply. In no event shall the Royal Society of Chemistry be held responsible for any errors or omissions in this Accepted Manuscript or any consequences arising from the use of any information it contains.

COMMUNICATION

Fast and Efficient Electrical-Thermal Responses of Functional Nanoparticles Decorated Nanocarbon Aerogels

Dong Xia^{a*}, Peng Huang^b, Heng Li^c and Noelia Rubio^dReceived 00th January 20xx,
Accepted 00th January 20xx

DOI: 10.1039/x0xx00000x

Joule heating characteristics of functional nanoparticles decorated nanocarbon aerogels are systemically investigated in terms of electrical-thermal responses. Studies verify that nanocarbon aerogels are exceptional supporting and electric-conducting monolithic frameworks for nanoparticles, enabling stable and accurate aerogel temperature control via direct electrical heating of the nanocarbon support, thus will find important values in electro-catalysis, energy storage, carbon capture and sorption applications.

Graphene oxide (GO) and oxidized carbon nanotube (oCNT) are superlative nanocarbon materials with large surface areas, excellent mechanical properties, outstanding hydrophilicity, promising water processabilities, tunable C/O ratios, and ultralight weight.^{1, 2} When assembled into three-dimensional (3D) nanocarbon aerogels (e.g. GO aerogels and oCNT aerogels), they possess additional promising features, such as hieratical internal microstructures and microchannels, tailored porosities, flexible mechanical compressibilities and stable support frameworks. As such, these 3D nanocarbon aerogels have found wide-ranging applications in catalysis, environmental remediation, sensors, electronics, energy storage, etc.³⁻⁵ After thermal reductive treatments, the graphiticity of the aerogels can be restored by eliminating the oxygen-containing functional groups in the nanocarbon structure, imparting them excellent electrical and thermal conductivities, the prerequisite for executing Joule heating experiments.^{6, 7} Currently, most published work related to Joule heating are focused on nanocarbon fibres or films,^{8, 9} very few studies have applied resistive electrical heating for nanocarbon aerogels.

Over recent years, inorganic nanoparticles have attracted great attention in multiple application fields, such as catalysis, adsorption, optoelectronic nanodevices, and carbon capture.

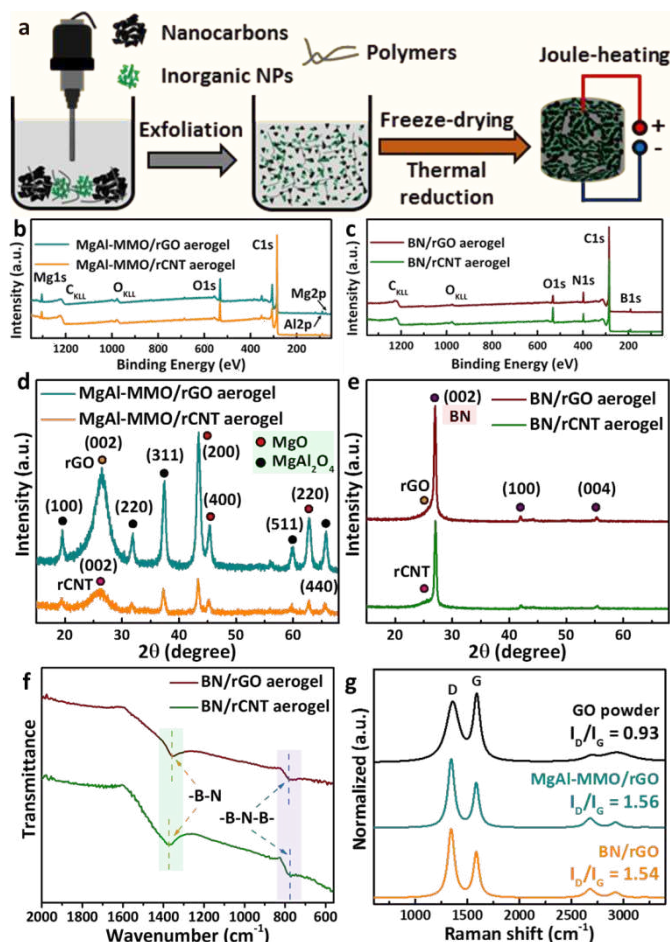


Fig. 1 (a) Schematic representation of the preparation of the hybrid NPs/rNanocarbon aerogels. (b-c) XPS full spectra, (d-e) XRD patterns of the MgAl-MMO/rGO, MgAl-MMO/rCNT, BN/rGO and BN/rCNT aerogels. (f) IR spectra of BN/rGO and BN/rCNT aerogels. (g) Raman spectra of the pristine GO powder, MgAl-MMO/rGO aerogel and BN/rGO aerogel.

Nevertheless, their applications are substantially hindered by the difficulty in regenerating exhausted nanoparticles, which either wastes large amounts of organic solvents or consumes considerable energy. These problems can be addressed by embedding the nanoparticles within the 3D network of the nanocarbon aerogel, with even better performances and stability. Enabled by the nanocarbon support framework, the

^a School of Chemistry, University of Leeds, Leeds, LS2 9JT, UK

^b School of Engineering and Physical Science, Heriot-Watt University, Edinburgh, EH14 4AS, UK

^c Key Laboratory of Estuarine Ecological Security and Environmental Health, Tan Kah Kee College, Xiamen University, 363105, Zhangzhou, China

^d Department of Chemistry and Materials, Imperial College London, SW7 2AZ, UK
Electronic Supplementary Information (ESI) available: [details of any supplementary information available should be included here]. See DOI: 10.1039/x0xx00000x

hybrid aerogel can be local resistive heated to desired temperatures at very fast heating rates, with precise temperature control and very little energy consumption. It is well known that nanocarbon aerogels are electrically and thermally stable during Joule heating,^{6, 10} but how these properties will be affected by the decoration of different functional nanoparticles (NPs) onto the nanocarbon aerogels, especially at high loadings, are largely unknown. In this study, mixed metal oxides (MMO) and boron nitride (BN), widely used adsorbents and catalysts,^{11, 12} were decorated onto rGO and rCNT aerogels at high loading fractions (up to 64 wt%, see TGA results in ESI, Fig. S1), to investigate their impact on the Joule heating characteristics of the nanocarbon aerogels, including electrical-thermal responses, heating/cooling kinetics, and thermal stabilities.

A wet-chemical approach to decorate MgAl-MMO and BN NPs onto nanocarbon aerogels were adopted in this study, as described in Fig. 1a.⁷ Specifically, the mixture of nanocarbons, inorganic NPs, and polymers are well dispersed in solution using ultra-sonication, followed by freeze-drying and thermal reduction to obtain different hybrid NPs/rNanocarbon aerogels (e.g. MgAl-MMO/rGO aerogel, BN/rGO aerogel, MgAl-MMO/rCNT aerogel and BN/rCNT aerogel). After thermal treatments, the graphiticity of the cylindrically monolithic nanocarbon aerogels is restored and can be directly connected to electrodes for Joule-heating studies, due to its excellent electrical conductivity (Fig. 1a, detailed Joule-heating procedures see ESI Fig. S2-S4) and good mechanical properties (ESI Fig. S5). XPS full spectra confirm that only C, O, Mg and Al elements exist in the MgAl-MMO/rGO and MgAl-MMO/rCNT aerogels (Fig. 1b), while the BN/rGO and BN/rCNT aerogels only possess C, O, B and N elements (Fig. 1c, detailed element atomic weight ratios see ESI Table S1). XRD patterns in Fig. 1d confirm that MgAl-MMO NPs are in the form of MgO and MgAl₂O₄ in both the hybrid rGO and rCNT aerogels, which have great potential to be used as adsorbents for carbon capture.¹³ The prominent diffraction peaks (002) in the MgAl-MMO/rGO and MgAl-MMO/rCNT aerogels are assigned to rGO aerogel¹⁴ and rCNT aerogel,¹⁵ respectively. For the BN/rGO aerogel and BN/rCNT aerogel, three pronounced characteristic diffraction peaks at 27°, 42° and 55° in Fig. 1e are attributed to the (002), (100) and (004) planes of typical hexagonal BN materials.¹⁶ As BN shares similar structure to graphene, their diffraction peaks will overlap at the same position, especially the (002) plane.¹⁷ However, re-assembly of the nanocarbon during thermal reduction results in larger interlayer distance than the typical graphite lattice structure, therefore, the asymmetric characteristic peak (002) at 25.6° in Fig. 1d is accredited to the nanocarbon.¹⁸ Two characteristic absorption bands appear in the IR spectra for both the BN/rGO aerogel and BN/rCNT aerogel (Fig. 1f), corresponding to the in-plane -B-N stretching vibration (~1360 cm⁻¹) and out-of-plane -B-N-B- bending vibration (~781 cm⁻¹) of BN materials,¹⁹ further confirming that the BN powders are well-combined with the aerogel supports (details of high-resolution XPS C1s, Mg1s, Al2p, B1s and N1s peaks see ESI Fig. S6). A significantly increased I_D/I_G ratio in the Raman spectra (Fig. 1g) for the rGO aerogels indicates the

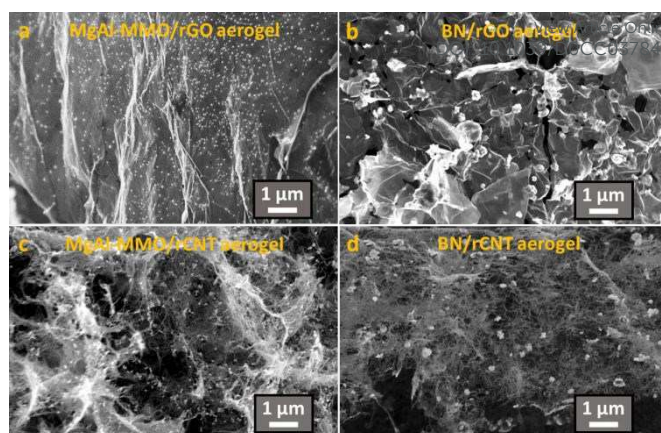


Fig. 2. SEM micrographs of MgAl-MMO/rGO aerogel (a), BN/rGO aerogel (b), MgAl-MMO/rCNT aerogel (c), and BN/rCNT aerogel (d).

formation of a large number of small-sized sp² hybridized domains within the structure.²⁰ Almost identical I_D/I_G ratios are observed for the MMO/rGO aerogel (I_D/I_G = 1.56) and BN/rGO aerogel (I_D/I_G = 1.54), suggesting that the decoration of NPs have no impact on the rGO sheets after thermal reduction (similar results for the rCNT aerogel, see Fig. S7).

SEM micrographs of the rGO and rCNT hybrid aerogels present distinct morphologies with interconnected flat rGO sheets and entangled rCNT fibres (Fig. 2 and Fig. S8). The MgAl-MMO and BN NPs are evenly anchored on the surface of the rGO sheets (Fig. 2a and Fig. 2b), whereas the MgAl-MMO and BN NPs are compactly attached within the rCNT strands, forming hieratical microstructures (Fig. 2c and Fig. 2d). As expected, the large surface area of the nanocarbon aerogels facilitates uniform distribution of NPs across the entire surface of the nanocarbon microstructures even at high loadings. EDX mapping confirms that only C, O, Mg and Al elements exist in the MgAl-MMO/rGO aerogels (in line with XPS results, Fig. 1b). These elements are densely and uniformly distributed on the aerogel surface (see ESI, Fig. S9), contributing to the key functionalities. Importantly, the interconnected structure of the conductive nanocarbon enables local resistive heating (Joule heating) and seamlessly conduction of heat across the 3D aerogel monolith, allowing the embedded insulating MgAl-MMO and BN NPs to be heated simultaneously.

To validate the above-mentioned assumptions, Joule heating experiments of MgAl-MMO/rGO, BN/rGO, MgAl-MMO/rCNT and BN/rCNT aerogels were performed. The hybrid aerogels exhibit excellent electrical conductivities despite the presence of high loadings of electrically insulating MgAl-MMO and BN nanoparticles (see ESI, Table S2), consistent with the interconnected structure of the nanocarbon network observed in the SEM micrographs. Due to the high porosity,²¹ all the nanocarbon aerogels are ultralight in weight, as supported by their low-density values. At a heating power of 2W, the MgAl-MMO/rCNT aerogel shows a higher Joule heating capacity (core temperature: 161 °C) than that of the MgAl-MMO/rGO aerogel (core temperature: 134 °C). This is caused by the more than 100% lower thermal conductivity of the MgAl-MMO/rCNT aerogel (0.095 W·m⁻¹·K⁻¹), coupled with its lower electrical conductivity and slower heat convection to the ambient

surroundings (condenser pore structure, see ESI). Compared with the MgAl-MMO decorated nanocarbon aerogels, both the BN/rGO aerogel and the BN/rCNT aerogel exhibit slightly lower Joule heating temperatures, in line with their relatively low electrical and high thermal conductivities.²²

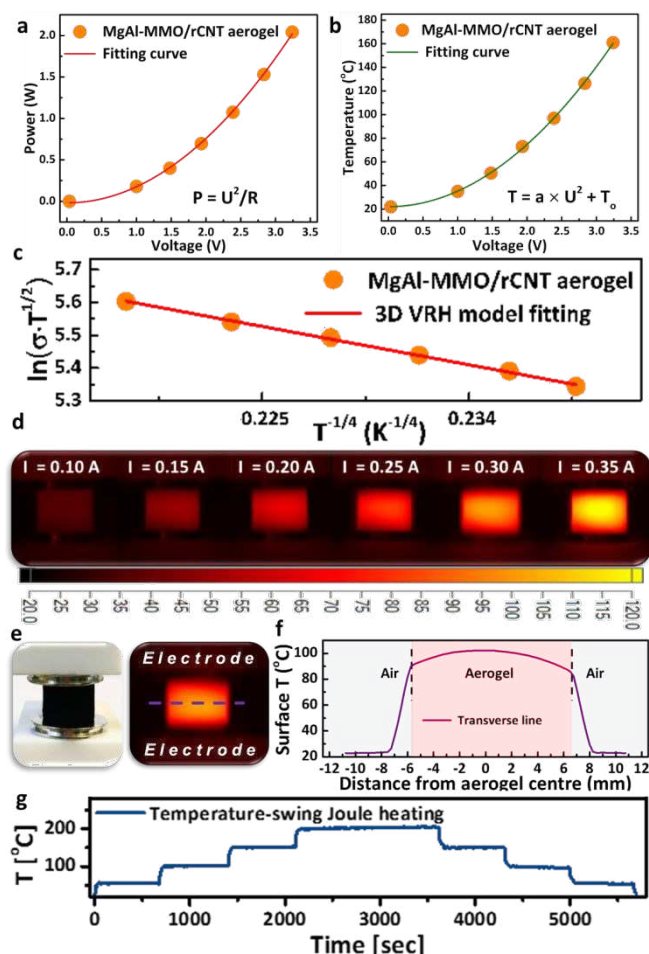


Fig. 3. Joule-heating voltage versus power input (a) and temperature (b) of the MgAl-MMO/rCNT aerogel. (c) Fit of 3D VRH model, that is $\ln(\sigma \cdot T^{-1/2})$ versus $T^{-1/4}$. (d) Thermal images of Joule heating of MgAl-MMO/rCNT aerogel at different electrical currents. (e) Digital photo of the MgAl-MMO/rCNT aerogel and the corresponding thermal image at $I = 0.30$ A. (f) Temperature distribution profile of Joule heating of MgAl-MMO/rCNT aerogel at $I = 0.30$ A. (g) Temperature-swing Joule heating of the MgAl-MMO/rCNT aerogel.

Considering its excellent electrical-thermal performance, the MgAl-MMO/rCNT aerogel was taken forward to investigate the Joule heating induced temperature distributions across the bulk of the material. The Joule-heating voltage and power of the hybrid aerogel follows well with Ohm's law ($P = U^2/R$), suggesting good stability of the conductive aerogel (Fig. 3a, I - P , I - T , and I - U curves during Joule-heating see ESI Fig. S10). In addition, a good fit of the Joule-heating temperature and voltage using the quadratic function equation ($T = a \times U^2 + T_0$, $a = 13.2$ °C/ V^2 , $T_0 = 22$ °C, Fig. 3b), indicates the complete conversion of electrical energy to thermal energy, highlighting the exceptional electrothermal efficiency of the nanocarbon supports.^{23, 24} The established temperature and voltage relationship enables the estimation of the Joule heating temperature of the hybrid aerogels by simply tuning the voltage

or powder input (ESI Fig. S11). In order to better understand the electrical conductivity of the hybrid aerogel, the results have been fitted with the 3D variable range hopping (VRH) model: $\sigma(T) = \sigma_0 \cdot T^{-1/2} \cdot \exp(-(T_0/T)^{1/4})$, here σ is the electrical conductivity (S/m); σ_0 is the electrical conductivity prefactor; T_0 is the temperature coefficient and T is the Joule heating temperature. The fitting result exhibits a pronounced linear relationship with $R^2 > 0.998$ (Fig. 3c),²⁵ suggesting the excellent electrical conductivity throughout the entire 3D aerogel structure. Similar electrical conduction behaviour has also been observed in the other hybrid aerogels (see ESI Fig. S12). Fig. 3d shows the infrared thermal images of the MgAl-MMO/rCNT aerogel under Joule heating. The temperature of the hybrid aerogel rises proportionally with the increase of the electrical current. A uniform temperature distribution profile is obtained across the entire aerogel surface, corroborated by the 3D VRH model fitting. Similar behaviour has been reported for the pure nanocarbon aerogels^{6, 10}, which implies that the high loading of the inorganic insulators has no detrimental effects on the electrical-thermal properties of the aerogel. Besides in direct contact with the air atmosphere, the hybrid aerogel exhibits very uniform temperature distribution across the whole cylindrical geometry, with only minor temperature variation from the centre to the edge (Fig. 3e-3f). Further apart from the edge of the aerogel (~ 2 mm), the temperature drops significantly to ambient temperature, due to thermal convection with the surrounding air atmosphere.⁶ Taking advantage of the special electrical-thermal characteristic, the temperature of the aerogel can be quickly and precisely tuned from ambient temperature to 200 °C via conveniently changing the power input, as demonstrated by the temperature-swing Joule heating of the nanocarbon aerogel (Fig. 3g). Importantly, all the prepared aerogels in this work, including MgAl-MMO/rGO, BN/rGO, MgAl-MMO/rCNT and BN/rCNT, exhibit similar temperature-swing behaviour, crucial for nanoparticles regeneration via local resistive heating (ESI Fig. S13-S16).

To investigate the electrical-thermal stability of the hybrid aerogels, Joule heating measurements are performed under repeated heating and cooling cycles. Although the hybrid aerogels display different heating capacities at the same Joule heating power input, all their cycling abilities are exceedingly stable even after 10 cycles (Figs. 4a-4d). Similarly, the Joule heating temperature and voltage of the aerogel under repeated thermal cycling are monitored. From both these results, there is no obvious change for each aerogel after 10 thermal cycles, which shows that the thermal cycling has no impact on the electrical conductivity of the aerogel (Fig. 4e-4f). In terms of the heating/cooling kinetics, all the hybrid aerogels exhibit exceptional performances (Fig. 4g), with heating rates of up to 580 K/min (622 K/min for cooling, see thermal images of a heating MgAl-MMO/rGO aerogel in ESI Fig. S17 and Table S3), outperforming most reported external heating/cooling approaches.^{26, 27} When the rGO aerogel is used as the support framework, no significant differences are observed for the heating efficiency of the MgAl-MMO/rGO and the BN/rGO aerogel (Fig. 4h). However, for the rCNT aerogel support framework, the BN/rCNT aerogel shows 69% lower heating

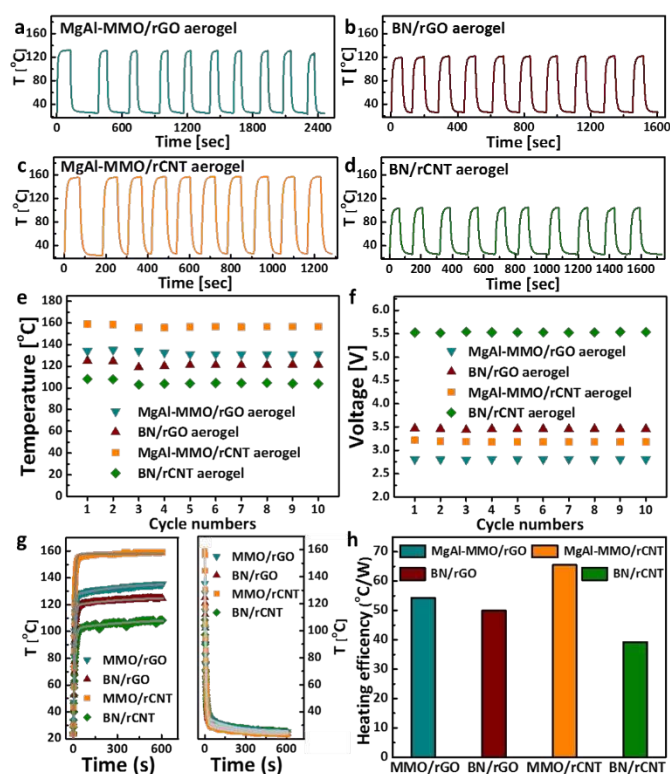


Fig. 4 (a-d) Joule heating cycles at 2W of as-prepared hybrid aerogels. (e-f) Temperature and voltage at different cycles of the corresponding hybrid aerogels. (g) Heating/cooling curves and (h) heating efficiency of the as-prepared hybrid aerogels at Joule heating of 2W.

efficiency than that of the MgAl-MMO/rCNT aerogel. This is because the BN/rCNT aerogel has a relatively high thermal conductivity, which leads to substantial convection heat transfer with the surrounding air atmosphere (ESI Table S2). The above results indicate that high loadings of various functional inorganic nanoparticles can be incorporated into the nanocarbon aerogels, with no significant impact on the electrical-thermal properties, opening up new routes for important applications, such as heterogeneous catalytic reactions, piezoelectronics and energy storage.

In summary, this work provides a universal and straightforward wet-chemical synthetic approach to fabricate highly porous, electrically-heatable hybrid nanocarbon aerogels with high loadings of functional inorganic nanoparticles. The electrical-thermal properties of the hybrid aerogels are not significantly affected by the presence of the insulating inorganic particles. Joule heating experiments show that the hybrid aerogels are thermally stable, and heat can be conducted seamlessly across the entire geometry through the interconnected structure. The temperature of the conductive aerogels can be accurately controlled by changing the power input. Electrical framework heating allows for regeneration of exhausted inorganic nanoparticles at very short time scales and low energy consumption. The facile synthetic approach and performance advantage of the nanoparticle/nanocarbon aerogel hybrids will be of great value in a wide range of application fields, including heterogeneous catalysis, sensing, electro-catalysis, and pre-combustion CO₂ capture.

Conflicts of interest

There are no conflicts to declare.

Notes and references

- A.J. Clancy, M.K. Bayazit, S.A. Hodge, N.T. Skipper, C.A. Howard and M.S. Shaffer, *Chem. Rev.*, 2018, **118**, 7363-7408.
- M. Khan, M.N. Tahir, S.F. Adil, H.U. Khan, A.A. Al-Warthan and W. Tremel, *J. Mater. Chem. A*, 2015, **3**, 18753-18808.
- N. Yousefi, X. Lu, M. Elimelech and N. Tufenkji, *Nat. Nanotechnol.* 2019, **14**, 107-119.
- E. Garcia-Bordeje, S. Víctor-Román, O. Sanahuja-Parejo, A.M. Benito and W.K. Maser, *Nanoscale*, 2018, **10**, 3526-3539.
- K.H. Kim, M.N. Tsui and M.F. Islam, *Chem. Mater.*, 2017, **29**, 2748-2755.
- R. Menzel, S. Barg, M. Miranda, D.B. Anthony, S.M. Bawaked, M. Mokhtar, S.A. Al-Thabaiti, S.N. Basahel, E. Saiz and M.S. Shaffer, *Adv. Funct. Mater.*, 2015, **25**, 28-35.
- D. Xia, H. Li, P. Huang, J. Mannering, U. Zafar, D. Baker and R. Menzel, *J. Mater. Chem. A*, 2019, **7**, 24027-24037.
- Y. Yao, F. Jiang, C. Yang, K. K. Fu, J. Hayden, C.F. Lin, H. Xie, M. Jiao, C. Yang and Y. Wang, *ACS Nano*, 2018, **12**, 5266-5273.
- S.H. Noh, W. Eom, W. J. Lee, H. Park, S. B. Ambade, S. O. Kim and T. H. Han, *Carbon*, 2019, **142**, 230-237.
- Q. Zhang, B. Zhang, Y. Yu, K. Zhao, P. He and B. Huang, *J. Mater. Sci.*, 2018, **53**, 528-537.
- R. Menzel, D. Iruetagoiena, Y. Wang, S.M. Bawaked, M. Mokhtar, S.A. Al-Thabaiti, S.N. Basahel and M.S. Shaffer, *Fuel*, 2016, **181**, 531-536.
- P. Wu, W. Zhu, Y. Chao, J. Zhang, P. Zhang, H. Zhu, C. Li, Z. Chen, H. Li and S. Dai, *Chem. Commun.*, 2016, **52**, 144-147.
- Y. Gao, Z. Zhang, J. Wu, X. Yi, A. Zheng, A. Umar, D. O'Hare and Q. Wang, *J. Mater. Chem. A*, 2013, **1**, 12782-12790.
- Z. Luo, C. Tan, X. Zhang, J. Chen, X. Cao, B. Li, Y. Zong, L. Huang, X. Huang and L. Wang, *Small*, 2016, **12**, 5920-5926.
- X. Zhang, J. Liu, B. Xu, Y. Su and Y. Luo, *Carbon*, 2011, **49**, 1884-1893.
- N. I. Kovtyukhova, N. Perea-López, M. Terrones and T.E. Mallouk, *ACS Nano*, 2017, **11**, 6746-6754.
- W. Luo, Y. Wang, E. Hitz, Y. Lin, B. Yang and L. Hu, *Adv. Funct. Mater.*, 2017, **27**, 1701450.
- C. Li, Q. Fu, K. Zhao, Y. Wang, H. Tang, H. Li, H. Jiang and L. Chen, *Carbon*, 2018, **139**, 1117-1125.
- L. Lu, J. He, P. Wu, Y. Wu, Y. Chao, H. Li, D. Tao, L. Fan, H. Li and W. Zhu, *Green Chem.*, 2018, **20**, 4453-4460.
- L.C. Spangler, J.P. Cline, J.D. Sakizadeh, C.J. Kiely and S. McIntosh, *Green Chem.*, 2019, **21**, 4046-4054.
- X. Hu and J. Zhu, *Adv. Funct. Mater.*, 2020, **30**, 1907234.
- F. An, X. Li, P. Min, H. Li, Z. Dai and Z.Z. Yu, *Carbon*, 2018, **126**, 119-127.
- R. Wang, Z. Xu, J. Zhuang, Z. Liu, L. Peng, Z. Li, Y. Liu, W. Gao and C. Gao, *Adv. Electron. Mater.*, 2017, **3**, 1600425.
- S. Tian, P. He, L. Chen, H. Wang, G. Ding and X. Xie, *Chem. Mater.*, 2017, **29**, 6214-6219.
- B. Román-Manso, S.M. Vega-Díaz, A. Morelos-Gómez, M. Terrones and M. Belmonte, *Carbon*, 2014, **80**, 120-126.
- W. Zhang, Q.Q. Kong, Z. Tao, J. Wei, L. Xie, X. Cui and C.M. Chen, *Adv. Mater. Interfaces*, 2019, **6**, 1900147.
- S. Barg, F.M. Perez, N. Ni, P. do Vale Pereira, R.C. Maher, E. Garcia-Tunon, S. Eslava, S. Agnoli, C. Mattevi and E. Saiz, *Nat. Commun.*, 2014, **5**, 4328.

Table of Contents

View Article Online
DOI: 10.1039/D0CC03784B

We report multifunctional nanoparticle/nanocarbon hybrid aerogels for effective and energy-efficient regeneration of exhausted functional nanoparticles.

